Persulfate activation by reduced graphene oxide membranes: practical and mechanistic insights concerning organic pollutants abatement

Alberto Cruz-Alcalde [a,*], Núria López-Vinent [a], Rui S. Ribeiro [b], Jaime Giménez [a], Carme Sans [a], Adrián M.T. Silva [b]

[a] *Department of Chemical Engineering and Analytical Chemistry, Faculty of Chemistry, Universitat de Barcelona, C/Martí i Franqués 1, 08028 Barcelona, Spain.*

[b] *Laboratory of Separation and Reaction Engineering - Laboratory of Catalysis and Materials (LSRE-LCM), Faculdade de Engenharia, Universidade do Porto, Rua Dr. Roberto Frías, 4200-465 Porto, Portugal.*

*Corresponding author: alberto.cruz@ub.edu

Abstract

The application of commercial, unmodified reduced graphene oxide (rGO) membranes for persulfate (PS) activation was assessed for the first time in this study through catalytic experiments performed in continuous mode. Phenol (Ph; C_0 = 5 mg L^{-1}) and venlafaxine (VFX; C_0 = 250 μg L^{-1}) were employed as model of phenolic pollutants and contaminants of emerging concern, respectively. The influence of the main operating parameters was first investigated considering an operation period of 24 h. For a rGO membrane with an effective area of 2.1 cm^2, contaminant removal is favored at lower flow rates (0.1 mL min^{-1}) and higher catalyst loads (15 mg). Assays carried out under these conditions yielded average removals of 90 and 94% for Ph and VFX, respectively, corresponding to normalized removal rates in the range of 1.71-1.79 L m^{-2} h^{-1} mg_{cat}^{-1}. Membrane stability

tests were conducted in continuous mode for 1 week, allowing to observe a significant catalyst deactivation after 2-3 d of operation, although the catalytic activity could be recovered through simple thermal regeneration procedures. Batch mode oxidation tests employing powder rGO treated at different temperatures (500, 850 and 1000 ºC) and materials characterization data allowed to conclude that a shift of the surface chemistry character from acidic to basic enhances the catalytic performance. Moreover, scavenging tests indicated that singlet oxygen ($^1O_2$), apparently generated by nucleophilic attack of PS to C=O in pyrone-like functionalities, is the main oxidizing species in the rGO-PS system.

Keywords: Water and wastewater treatment; graphene derivatives; catalytic membranes; persulfate activation; singlet oxygen.

1. Introduction

Graphene-based materials have been used in activated persulfate oxidation as supports for metal catalysts, both in powder [1,2] and membrane [3,4] form. Nevertheless, owing to their unique electronic properties [5], several works have already reported the use of metal-free graphene derivatives for persulfate (PS) or peroxymonosulfate (PMS) activation and subsequent removal of organic pollutants from water, avoiding the use of metals. Most of these studies focused on the doping of graphene oxide (GO) with different heteroatoms, mainly nitrogen alone [6–15] or in combination with others such as sulfur [16–18], boron or phosphorus [19]. The modification of these materials improves catalytic activities by the presence of the newly introduced atoms and related chemical groups. However, a mere reduction in the oxygen content may also convert GO into a suitable activator for PS and PMS. In this regard, Sun and coworkers reported the first

demonstration of the superior effectivity of a reduced GO (rGO) in PMS activation when compared to other carbon materials [20]. Subsequent publications confirmed it, providing also evidences for PS activation [21–24]. Thus, rGO can be considered a material of practical interest in this application, as complex, expensive and time-consuming doping procedures may be replaced by a simple thermal or hydrothermal reduction of GO.

It is well known that one of the main drawbacks of heterogeneous catalytic oxidation is the need of an additional step to recover the catalyst from the treated water. In this sense, the use of catalytic membranes is expected to be advantageous, as the recovery stage required when catalysts are used in the form of particles is saved. To the best of the authors' knowledge, there are only four documents in the literature reporting the use of metal-free carbon-based catalytic membranes for activation of PS, all of them containing rGO-based materials [25–28]. This can be explained by the 2D nature of graphene-based materials [29], which is a crucial feature to fabricate mechanically stable, smooth, carbon-based catalytic membranes. rGO was doped with nitrogen in three of these previous works [25–27], and assembled with multi-walled carbon nanotubes (MWCNTs) in the other study [28]. Therefore, the application of catalytic membranes prepared with unmodified rGO for PS activation has not been reported yet. In addition, there is a lack of information on the influence of basic operation parameters for catalytic membranes operated in continuous mode (i.e., catalyst load and flow rate). Furthermore, the operation periods previously studied have been mostly limited to relatively short time intervals (i.e., $\leq$ 6.5 h in 3 of the 4 published studies).

The reaction mechanisms linked to the observed activity in the rGO-PS/PMS system are still to be clarified for the complete understanding of the process. Although both radical ($HO^{\bullet}$, $SO_4^{\bullet-}$) and non-radical pathways appear to be possible, studies on rGO-PS/PMS oxidation mechanisms often report conflicting results. Some works claim that $HO^{\bullet}$ is the

main oxidizing species with some contribution of $SO_4^{\bullet -}$ [21]. According to others, $SO_4^{\bullet -}$ is the dominant species and HO• contributes to a lower extent [22]. Alternatively, some authors have concluded that a non-radical mechanism constitutes the prevailing reaction pathway [24,30], in which case the role of singlet oxygen ($^1O_2$) may be important [24]. Bearing this in mind, it is evident that additional studies are required to clarify which are the main oxidizing species. Concerning the main activation sites on rGO, a correlation has been observed between improved PMS activation and a higher proportion (among oxygen functionalities) of carbonyl surface groups (C=O) [31]. This suggests that ketonic moieties can be the main activation sites, a hypothesis supported by quantum chemical calculations on amorphous carbonaceous models [32]. However, a direct experimental confirmation of these simulation results is still required.

The main goal of this work is to study the performance of catalytic membranes, prepared by vacuum filtration of undoped rGO powder into a polytetrafluoroethylene (PTFE) support, in PS activation and organic pollutants oxidation in continuous mode of operation. To that end, the influence of the catalyst load and the water flow rate on the process efficiency, as well as the long-term performance of the membrane, were studied for the first time. Phenol (Ph) and venlafaxine (VFX) were used as target pollutants. PS was chosen over PMS because of its higher chemical stability and lower cost [33,34]. Another important objective was to investigate the mechanism of PS activation by rGO. In this way, the combination of scavenging tests and catalytic oxidation experiments employing rGO powder treated at different temperatures were used to propose a mechanism for PS activation by rGO.

2. Materials and methods

2.1. Chemicals and reagents

The chemicals, reagents and water matrices used in this study are described in Text S1 and Table S1.

2.2. Graphene-based materials

Commercially available reduced graphene oxide (rGO) was the material employed as catalyst. It was acquired from Sigma-Aldrich, Germany (ref. 796034), and used in both preliminary batch tests and to fabricate the membranes used in experiments performed in continuous mode of operation. To investigate the mechanism of PS activation, three other materials were prepared by thermal treatment of rGO under a N_2 flow (100 cm^3 min^{-1}) in a ThermoLab vertical oven, at different temperatures (i.e., 500, 850 and 1000 ºC). In a first treatment step, which was common to all the materials prepared, rGO was treated at 120 ºC during 60 min. This temperature was reached through a heating ramp of 2 ºC min^{-1}. Then, a second treatment step was performed at different temperatures. A heating ramp of 2 ºC min^{-1} was set up to reach 500, 850 and 1000 ºC. These temperatures were kept for 30 min. The materials prepared in this way were denoted as rGO-500, rGO-850 and rGO-1000, and employed in experiments performed in batch mode.

2.3. *Materials characterization*

Textural properties of rGO and derived materials were determined from N_2 adsorption-desorption isotherms at -196 ºC, in particular the specific surface area (S_{BET}), as described in a previous publication [35]. Thermogravimetric analysis (TGA) was performed in a Netzsch STA 490 PC/4/H Luxx thermal analyser, where the powder sample was heated

in a gas flow from 50 to 1000 ºC at 10 ºC min^{-1}. Both inert (N_2) and oxidative (air) gas flows were employed.

Temperature programmed desorption (TPD) was performed in a fully automated AMI-300 Catalyst Characterization Instrument (Altamira Instruments), equipped with a quadrupole mass spectrometer (Dymaxion, Ametek), as described elsewhere [36]. The amounts of CO_2 and CO were obtained by integrating the area of the respective spectra. Deconvolution analysis of the CO_2 and CO TPD spectra was performed using a well-established procedure [36,37]. Accordingly, the peaks in the CO_2 TPD spectra were assigned to different functional groups, namely: strongly acidic carboxylic acids (SA), less acidic carboxylic acids (LA), carboxylic anhydrides (CAn), and lactones (Lac). Likewise, the peaks in the CO TPD spectra were assigned to carboxylic anhydrides (CAn), phenols (Ph), carbonyls and quinones (CQ) and basic surface groups (Bas), such as pyrones and chromenes. In the CO_2 spectra, the width at half-height (W) was taken the same for CAn and Lac; in the CO spectra, the same W was considered for Ph and CQ whenever peak shoulders were unclear.

2.4. Catalytic oxidation experiments

Two different operation modes were used in rGO-PS oxidation experiments: batch and continuous mode. In batch experiments, 5 mg L^{-1} or 30 mg L^{-1} phenol solutions containing 0.25-1 mM of PS were prepared and placed in 8 mL amber glass bottles equipped with a stirring bar, which were employed as reactors. In some of these tests, *tert*-butanol (tBuOH), methanol (MeOH) or furfuryl alcohol (FFA) were also added in excess (100 mM) to act as scavengers for oxidizing species. An experiment under constant nitrogen bubbling (i.e., without the presence of dissolved oxygen) was in addition conducted. In general, experiments started with the addition under vigorous stirring of rGO (or

derivatives) powder at varying dosages (0.25-0.5 g L^{-1}). Samples were withdrawn at regular time intervals and filtered through 0.2 μm PTFE syringe filters. All batch catalytic assays were conducted for 90 min. In continuous flow experiments, rGO membranes (effective area: 2.1 cm^2) were tested in dead-end mode. These were prepared by vacuum filtration of aqueous rGO dispersions (0.2-0.5 g L^{-1}) into 0.2 μm Omnipore PTFE membranes, resulting in a supported amount of catalyst of 5-15 mg. Aqueous solutions of Ph (5 mg L^{-1}) or VFX (250 μg L^{-1}) containing 1 mM of PS were placed in a stirred glass flask and continuously fed to a glass membrane cell at a flow rate of 0.1-0.5 mL min^{-1}, by means of an Ismatec 829 peristaltic pump (Cole-Parmer, USA). Samples were collected from the filtrate at regular time intervals. In this case, experiments were conducted for at least 24 h, and up to 1 week (168 h). The protocol of the catalytic experiments performed in continuous mode with PTFE-supported rGO membranes and the experimental setup used for that purpose are detailed in Text S2 and Figs. S1 and S2. As described in Text S1 and Table S1, four water matrices were employed in the catalytic experiments, namely distilled water (DW), bottled water (BW), surface water (SW) and treated wastewater (WW). Regardless of the operation mode, all catalytic experiments were performed at room temperature (25 ºC) and the natural pH of the water matrix (i.e., without pH adjustment and in the absence of buffers). Nevertheless, the pH was monitored during all the experiments. In the case of tests with BW, SW and WW, the pH was unaffected during the experiments due to the natural buffer capacity of each matrix, whereas in experiments with DW the pH was only slightly reduced (i.e., from 7.0 ± 0.1, in the initial phenol solution, to 6.8 ± 0.2, in the treated water). Control experiments without the addition of PS were performed to evaluate the adsorption of Ph onto rGO and derived materials. The stability of Ph and VFX in PS solutions (i.e., without the presence

of rGO) was also tested. In all cases, samples were frozen after withdrawal and kept at these conditions until approximately 1 h before analysis.

2.5. Analytical techniques

Phenol was determined by High Performance Liquid Chromatography with ultraviolet detection (HPLC-UV), whereas Venlafaxine concentration was determined by HPLC with fluorescence detection. Detailed descriptions of the analytical methods, including quality assurance (QA) parameters, can be found in Text S3 and Tables S2 and S3. The concentration of persulfate was determined by the N,N-diethyl-p-phenylenediamine (DPD) colorimetric method [27]. Dissolved Organic Carbon (DOC) content was determined with a Shimadzu TOC-L analyzer.

3. Results and discussion

3.1. Materials characterization

rGO is a commercial multilayer material with 15-20 stacked graphene sheets (as described by the supplier) and a low ash content (TGA residue of *ca.* 1 wt.%; determined under oxidative atmosphere, as shown in Fig. S3a). Both the pristine rGO and derivatives of this material, obtained by thermal treatment at different temperatures and employed later on in this work for the mechanistic study of the process (Section 3.3), were characterized. The N_2 adsorption-desorption isotherms are given in Fig. S4, and the respective S_{BET} values are summarized in Table 1. As observed, all the materials have S_{BET} values in the range 262-281 $m^2\ g^{-1}$. Therefore, it can be concluded that the textural properties of the resulting materials are negligibly affected upon thermal treatment of rGO, regardless of the temperature employed. This is of utmost importance for this study,

since maintaining textural properties unaltered is crucial to elucidating the influence of surface chemistry in the catalytic properties.

The effect of the different thermal treatments on the surface chemistry properties of the graphene-based materials was investigated by TGA and TPD. The former allows determining the total volatile content, while the latter allows quantifying and identifying different oxygen-containing surface groups, which are released as CO_2 and CO upon heating [36,37]. The CO_2 and CO TPD spectra of the graphene-based materials are given in Figs. S5a and b, respectively. The total amount of surface groups released as CO_2 and CO (determined from the area under the TPD spectrum) and the corresponding oxygen content (calculated from the total amounts of CO_2 and CO released from the surface of the carbon materials), are summarized in Table 1.

Table 1. Specific surface area (S_{BET}), amount of volatiles (determined by TGA), amounts of CO_2 and CO released by TPD, and corresponding percentage of oxygen (assuming that all the surface oxygen is released as CO_2 and/or CO).

Material	S_{BET} ($m^2\ g^{-1}$)	Volatiles (wt.%)	[CO_2] ($\mu mol\ g^{-1}$)	[CO] ($\mu mol\ g^{-1}$)	O (wt.%)	CO/CO_2
rGO	266	14.9	1044	408	4.0	0.4
rGO-500	262	13.3	395	821	2.6	2.1
rGO-850	276	5.6	0	360	0.6	n.a.
rGO-1000	281	4.7	0	239	0.4	n.a.

n.a.: not applicable;.

The first conclusion to be withdrawn from the results given in Table 1 is that, despite the commercial material employed in this study was purchased as being GO, it can actually be described as a partially reduced GO (rGO), considering both its multilayer configuration (as mentioned above) and the relatively low surface oxygen content (4.0

wt.%, as determined by TPD). Notwithstanding, the amount of oxygen-containing surface groups decreases as the temperature of the thermal treatment increases. This trend becomes particularly clear when the oxygen content of the graphene-based materials is plotted against the temperature of the thermal treatment (Fig. 1a), obtaining a near linear correlation. This evolution is followed by the decrease of volatiles (Table 1). An illustrative example of the TGA performed for the determination of the volatile content of the materials is shown in Fig. S3b.

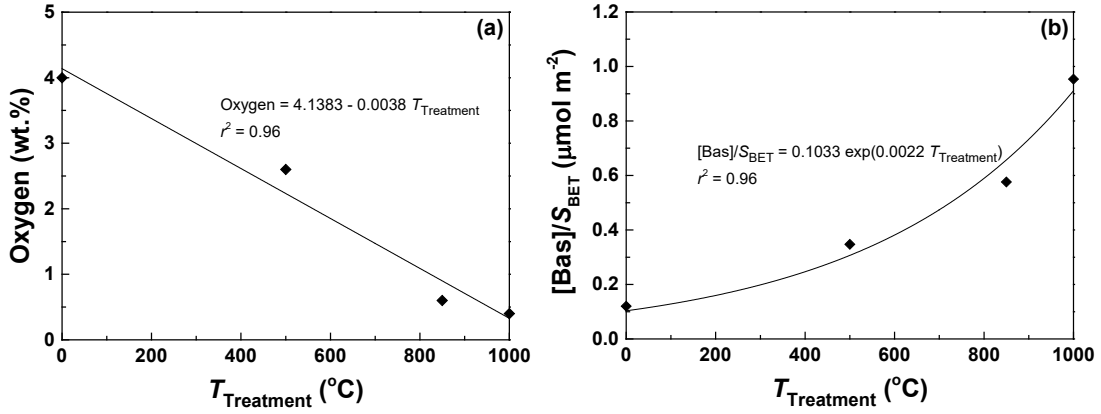

Figure 1. (a) Oxygen content and (b) [Bas]/S_{BET} as a function of the temperature employed in the thermal treatment ($T_{Treatment}$) of rGO. Points represent experimental data, while lines represent (a) linear and (b) exponential fittings.

Deconvolution analysis of the CO_2 and CO TPD spectra was performed as described in Section 2.4, in order to identify and quantify the functional groups originally present at the surface of rGO, as well as those removed and/or generated during the thermal treatments under the inert atmosphere of N_2. The deconvolution spectra are given in Fig. S6, the corresponding results being detailed in Tables S4 and S5, respectively. From these results, it can be concluded that the decrease of oxygen-containing groups, previously commented, is due to the selective removal of functionalities whose decomposition temperature is below that employed in the thermal treatment. For instance, all the strongly

acidic carboxylic acids (SA), originally released at around 248 ºC in the pristine rGO (Fig. S6a and Table S4), are removed upon thermal treatment at 500 ºC during 30 min (Fig. S6c). However, a fraction of less acidic carboxylic acids (LA), originally released at around 400 ºC, subsists after the thermal treatment. This phenomenon has already been reported in a study in which carboxylic acids were still detected by X-ray photoelectron spectroscopy (XPS) after thermal treatment of rGO at 400 ºC during 60 min [38]. Nevertheless, the results suggest that some of these less thermally stable groups are in fact converted into others with higher thermal resistance, such as those containing highly stable carbonyl and ether groups [39,40]. These chemical changes of oxygen-containing functional groups have been elucidated elsewhere [40], and are particularly evident in the case of basic surface groups (Bas), such as pyrones and chromenes, which decompose at the highest temperatures. Indeed, the amount of these functionalities increases almost exponentially as the temperature of the thermal treatment increases, as revealed when the concentration of Bas determined by TPD is normalized by the S_{BET} of the graphene-based materials (i.e., ([Bas]/S_{BET}), and represented as a function of the temperature employed in the thermal treatment (Fig. 1b). It is noteworthy that carbonyls and quinones (CQ) are still detected by TPD after thermal treatment at both 850 ºC and 1000 ºC (Figs. S5f and h and Table S5). This is in agreement with a previous study revealing the thermal resistance of these groups up to around 1230 ºC when embedded to graphene-based materials [40].

3.2. Performance of catalytic rGO membranes in activated PS oxidation

Experiments conducted in batch mode were first performed to test the activity of the commercial rGO in PS activation for the removal of phenol at 5 mg L^{-1}, under different catalyst (0.25-0.5 g L^{-1}) and oxidant (0.25-1 mM) dosages. Results are presented in Fig.

S7. Adsorption tests and controls without the addition of rGO (non-catalytic experiments) were also performed. No abatement of Ph was observed after 90 min in the presence of PS only (data not shown). Adsorption experiments revealed that the Ph removals increase as the dose of rGO increases, reaching maximum adsorption levels in the range between 20 and 60% of the initial Ph content (i.e. for 0.25 and 0.5 g rGO L^{-1}, respectively). Catalytic oxidation experiments showed that a great improvement in the removal efficiency is achieved upon addition of PS. This makes clear that the selected commercial rGO is an excellent activator for PS, in agreement with observations made in previous studies conducted with lab-synthetized rGO for the activation of PS [21,22]. Additional tests conducted in complex water matrices (i.e., bottled and surface water, and secondary treated wastewater) also revealed good Ph removal performances (see Fig. S7c).

After preliminary experiments in batch mode, the rGO membranes prepared by vacuum filtration over PTFE support were used in experiments performed in continuous mode for PS activation and removal of phenol at 5 mg L^{-1}. First, the influence of fundamental operational parameters on the process performance was studied. For that purpose, the PS concentration was kept at 1 mM in all cases. Different water flow rates (0.1, 0.25 and 0.5 mL min^{-1}) with 15 mg of catalyst in all cases and different amounts of supported rGO (1, 5 and 15 mg) at a constant flow rate of 0.1 mL min^{-1} were employed. Results for a total operation time of 24 h are shown in Fig. 2. For experiments conducted with different catalyst loads, a direct relation between the amount of rGO used and the Ph abatement was observed (Fig. 2a). Specifically, the average Ph removals observed throughout the entire operation period (i.e., 24 h) were 15, 62 and 90% for catalyst loads of 1, 5 and 15 mg L^{-1}, respectively. In general, it was observed that a transient state firstly appears during the first hours of operation until the maximum oxidation efficiency was reached, followed by a gradual decrease of the process performance for the remaining experimental period.

This behavior was specially observed in the case of experiments with 1 and 5 mg of supported rGO and was much less pronounced in the case of membranes containing the highest load (i.e., 15 mg) of catalyst. In this case, in fact, an almost steady removal of Ph of about 90% was observed in the period between 2 and 24 hours. Concerning tests at different water flow rates, the progressive loss of catalytic activity was not as clear as in the case of varying amounts of rGO. This may indicate that the amount of catalyst is a more critical parameter regarding catalyst deactivation. In this case, an inverse relation was observed between the flow rate and Ph abatement (Fig. 2b). The average removals observed throughout the entire operation period were 32, 67 and 90% for water flow rates of 0.5, 0.25 and 0.1 mL min^{-1}, respectively. Thus, the lower flow rate value tested (i.e., 0.1 mL min^{-1}) resulted in better activation efficiencies and therefore a higher and more sustained removal of Ph. This can be ascribed to the better contact between rGO and PS achieved under these conditions.

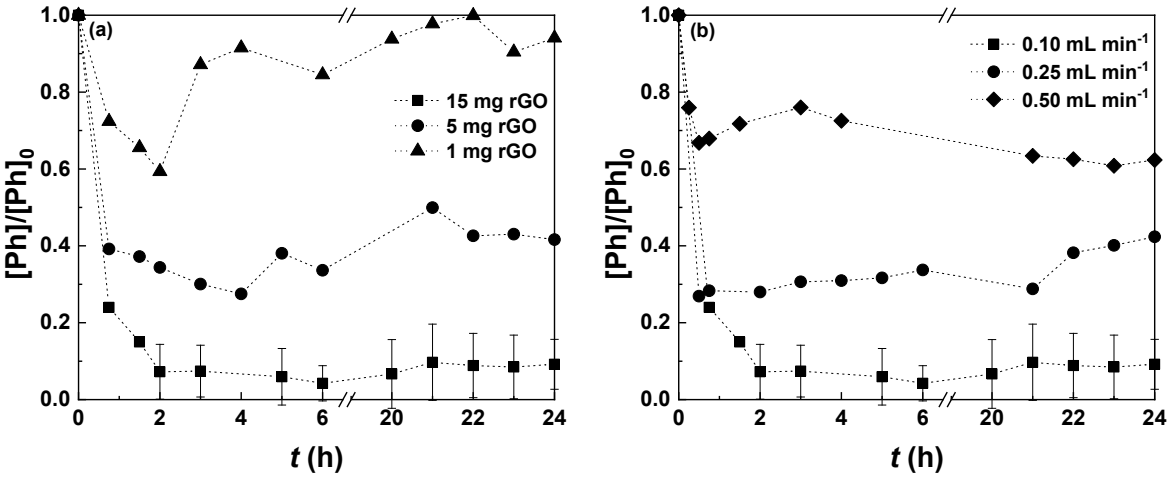

Figure 2. Phenol abatement in continuous mode experiments, in deionized water. $[Ph]_0$ = 5 mg L^{-1}, $[PS]_0$ = 1 mM, and pH_0 = 7.0 (inherent pH). a) Influence of the amount of catalyst supported (rGO = 1, 5 or 15 mg) at a flow rate = 0.1 mL min^{-1}. b) Influence of the flow rate (0.1, 0.25 or 0.5 mL min^{-1}) with 15 mg of supported rGO.

The PTFE-supported rGO membranes were also tested for the removal of VFX (C_0 = 250 μg L^{-1}), an antidepressant drug recently included in the 3rd revision of the Watch List of contaminants of emerging concern under the European Union Water Framework Directive [41]. For that purpose, an additional catalytic experiment was performed during 24 h under the optimum operation conditions (i.e., rGO dosage = 15 mg and flow rate = 0.1 mL min^{-1}, as previously determined). Results are shown in Fig. 3. Experiments performed in the absence of PS were also conducted to estimate the contribution of adsorption to the overall removal obtained in catalytic oxidation experiments with PS. As observed, a fast pollutant abatement is observed at an early stage of the adsorption experiments, followed by a gradual increase in its concentration at the system outlet. This decrease of the adsorption capacity can be ascribed to membrane saturation. On its part, oxidative VFX removal efficiency was very high and constant during the entire operation period, reaching a mean value as high as 94% of its initial content. These results confirm the effectivity and versatility of the rGO catalytic membrane for the activation of PS and degradation of structurally different water pollutants at different concentrations.

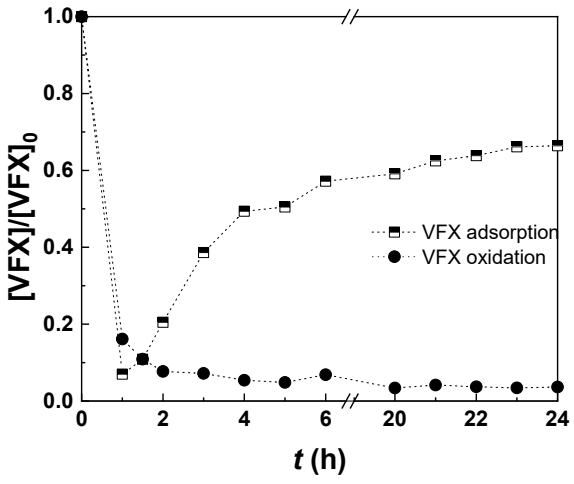

Figure 3. Oxidation and adsorption experiments for venlafaxine ($[VFX]_0$ = 250 μg L^{-1}) degradation using PTFE-supported rGO membranes tested in continuous mode, in distilled water. 24 h tests. $[rGO]_0$ = 15 mg, $[PS]_0$ = 1 mM, flow rate = 0.1 mL min^{-1}, and pH_0 = 7.0 (inherent pH).

The catalytic stability of the rGO membrane was further tested through experiments performed in continuous mode for a period of 1 week (168 h). A catalyst load of 15 mg and a flow rate of 0.1 mL min^{-1} were also employed, as these were the best performing conditions according to the previous screening of influential factors. Simultaneously, a separate control experiment without the presence of PS was also conducted for the same time period. Results are presented in Fig. 4. Relatively high removal levels of Ph were initially observed in the adsorption control test (as high as 40%), followed by a gradual decrease in the Ph removal efficiency through this mechanism. A steady $[Ph]/[Ph]_0$ value of 1 was observed after 3 days of operation, indicating that the membrane saturation was reached. Regarding the catalytic oxidation experiment with PS, very high Ph removals (> 90%) were observed during the first 48 h, although a slow but gradual decrease in the oxidation efficiency was observed after 24 hours of operation. The period from 48 to 72 h was characterized by a significant loss of the catalytic activity (from 90 to 60% of Ph removal), followed by an even stiffer drop within the following 24 h (from 60 to 0% of Ph removal). The evolution of remaining PS in the catalytic oxidation experiment, also shown in Fig. 4, is in agreement with the observed Ph abatement during the same operation period. Indeed, PS consumption was no longer observed from around 96 h onwards.

Deactivation of the rGO membrane can be explained by the increase of the amount of oxygen-containing functionalities, especially phenolic and carboxylic groups (as determined by TPD: Tables S4 and S5), explained by the adsorption of both Ph and its transformation products, as well as the oxidation of more reduced oxygen-containing functionalities in pristine rGO. Similar phenomena have been previously described in the literature, together with simple procedures aimed at catalyst regeneration that can be

useful also in the present case [21,30]. Further data and discussion on rGO deactivation causes and regeneration strategies can be found in the Supplementary Information (Text S4, Figs. S8-10 and Tables S4-S6).

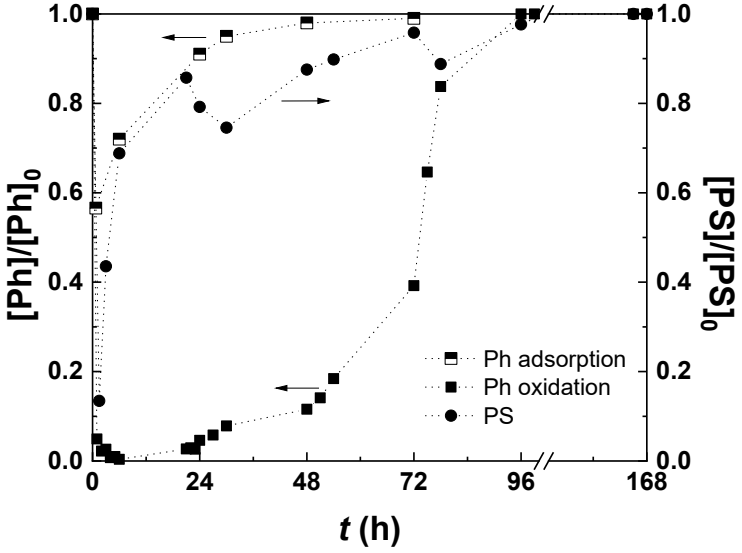

Figure 4. Oxidation and adsorption experiments for phenol degradation using PTFE-supported rGO membranes tested in continuous mode, in distilled water. 1-week test. $[Ph]_0$ = 5 mg L^{-1}, $[rGO]_0$ = 15 mg, $[PS]_0$ = 1 mM, flow rate = 0.1 mL min^{-1}, and pH_0 = 7.0 (inherent pH).

The results obtained in this study were compared to those previously reported in the literature which employed metal-free carbon-based membranes for activation of PMS or PS in continuous mode. The main features and results of the four works available to date are summarized in Table 2. All of them reported the use of modified reduced graphene oxide membranes prepared with different degrees of difficulty. Two of them were N-doped by hydrothermal or thermal methods at relatively high temperatures (180-350 ºC) and employing different nitrogen precursors [25,26]. In the two remaining works, N-doped rGO on one hand, and a hybrid material containing MWCNTs, on the other, were prepared by different hydrothermal and thermal methods and then mixed with polymeric materials to fabricate composite membranes [27,28]. In the present work, comparatively

much simpler catalytic membranes were prepared from a partially reduced commercial GO material (rGO). Performance comparison between studies was expressed as the average normalized removal rate, calculated as described in Eq. 1.

$$\text{Normalized removal rate} = \frac{Q}{A \cdot m_{\text{cat}}} \cdot \frac{C_{\text{in}} - C_{\text{out}}}{C_{\text{in}}} \quad (1)$$

where Q is the water flow rate passing through the membrane (L h^{-1}), A is the membrane effective area (m^2), m_{cat} is the catalyst load (mg_{cat}) and C_{in} and C_{out} are, respectively, the concentration of pollutant at the inlet and the outlet of the membrane. This figure is expressed in L m^{-2} h^{-1} mg_{cat}^{-1} and conceptually represents the flux of pollutant-free water per mass of catalyst. Operational and removal data required to calculate it was retrieved from the corresponding publications. Values of this metric were calculated as the average values for the entire operation period, taking into consideration measured residual concentrations of pollutants at each experimental point, and included in Table 2 to be used for comparison between works. The results indicate that the catalytic performance of the rGO membrane herein reported for Ph and VFX oxidation (1.71 and 1.79 L m^{-2} h^{-1} mg_{cat}^{-1}, respectively) falls within the same order of magnitude of the values calculated from previous results concerning the abatement of different pollutants (in the range of 0.89-3.76 L m^{-2} h^{-1} mg_{cat}^{-1}). Only in one of those studies this metric was found to be markedly higher for Ph removal (13.81 L m^{-2} h^{-1} mg_{cat}^{-1} [26]). However, the operation time in that study was only 6.5 h, compared to the 24 h in the present work. Extending this period up to 24 h is likely to reduce the catalyst activity and thus the average performance throughout the experiment. In any case, in view of values for this normalized metric in different catalytic membrane systems, it can be concluded that comparable performances were obtained in this work with respect to previous studies. This fact points

out the possibility of using membranes prepared through simpler procedures and thus save manufacturing costs by significantly reducing energy and chemical requirements. Another distinctive feature of the present study is the investigation of the influence of the main operating parameters, namely catalyst load and water flow rate. In this regard, three levels were tested for each factor and the best conditions used in the subsequent experiments. Only one of the previous works addressed this question, although no more than the influence of the catalyst load was investigated. A third aspect to highlight in the present study compared to the previous literature, is the extension of the operational period up to one week (i.e., up to 168 h), which allowed to better study the stability of the rGO membrane (Fig. 4). Most of the previous works tested the performance of the prepared membranes during a few hours (3-6.5 h), with only one reporting experimental periods of 24 h.

Table 2. Studies reporting the use of metal-free carbon-based membranes for activation of peroxymonosulfate (PMS) or persulfate (PS) in continuous mode, and degradation of water organic pollutants. All experiments were conducted at room temperature.

Ref.	Membrane description	Operating conditions	Pollutant	Pollutant removal	Normalized removal rate
Liu *et al*., 2016 [25]	**N-doped rGO** prepared by hydrothermal treatment of commercial GO with NH_3 at 180 ºC, dispersed in N-methyl-2-pyrrolidone (NMP) and vacuum filtered onto PTFE membrane (5 μm pore size)	Membrane weight = 15 mg (studied range: 5-15 mg) Q = 1.5 mL min^{-1} $[PS]_0$ = 238 mg L^{-1} $pH_{solution}$ = 6.5 t = 3 h	Phenol (47 mg L^{-1})	~80% (after 3 h)	3.76 L m^{-2} h^{-1} mg_{cat}^{-1} (average of 3 h)
Pedrosa *et al*., 2019 [26]	**N-doped rGO** prepared by thermal treatment of graphite oxide (Hummers' method) with melamine under 350 ºC air atmosphere, dispersed in NMP and vacuum filtered onto PTFE membrane (0.2 μm pore size)	Membrane weight = 15 mg Q = 1.5 mL min^{-1} $[PS]_0$ = 238 mg L^{-1} $pH_{solution}$ = natural pH (~7.0) t = 6.5 h	Phenol (5 mg L^{-1})	30% (after 6.5 h)	13.81 L m^{-2} h^{-1} mg_{cat}^{-1} (average of 6.5 h)
Sheng *et al*., 2020 [28]	**rGO–MWCNTs** prepared by hydrothermal treatment of commercial GO at 120 ºC, dispersed in water containing MWCNTs and copolymer pluronic F127 and vacuum filtered onto Nylon membrane (0.45 μm pore size)	Membrane weight = 13.9 mg Q = 1.0 mL min^{-1} $[PS]_0$ = 1190 mg L^{-1} $pH_{solution}$ = not reported t = 3 h	Sulfamethoxazole (500 μg L^{-1})	77% (after 3 h)	2.31 L m^{-2} h^{-1} mg_{cat}^{-1} (average of 3 h)
Vieira et al., 2020 [27]	**N-doped rGO–PVDF composite** prepared by thermal treatment of graphite oxide (Hummers' method) with melamine at 350 ºC under air atmosphere, then included in a PVDF matrix.	Membrane weight = 23 mg Q = 0.1 mL min^{-1} $[PS]_0$ = 25 mg L^{-1} $pH_{solution}$ = natural pH (5.9) t = 24 h	Ofloxacin, ciprofloxacin and enrofloxacin, simultaneously (100 μg L^{-1} each)	54, 77 and 91%, respectively (after 24 h)	0.89 (ofloxacin) 1.02 (ciprofloxacin) 1.19 (enrofloxacin) in L m^{-2} h^{-1} mg_{cat}^{-1} (average of 24 h)
This study	**Commercial rGO** dispersed in distilled water and vacuum filtered onto a PTFE membrane (0.2 μm pore size)	Membrane weight = 15 mg (studied range: 5-15 mg) Q = 0.1 mL min^{-1} (studied range 0.1-0.5 mL min^{-1}) $[PS]_0$ = 238 mg L^{-1} $pH_{solution}$ = natural pH (7.0) t = 24-168 h	Phenol (5 mg L^{-1}) Venlafaxine (250 μg L^{-1})	91, 88 and 61% (after 24, 48 and 72 h, respectively). 96% (after 24 h)	1.71 L m^{-2} h^{-1} mg_{cat}^{-1} (average of 24 h) 1.79 L m^{-2} h^{-1} mg_{cat}^{-1} (average of 24 h)

Data retrieved from Scopus database on April 21, 2021, using the following search: "Carbon AND membrane AND persulfate OR peroxymonosulfate".

3.3. *Mechanism of PS activation by rGO*

Additional experiments were performed in order to study the mechanism behind the rGO-PS oxidation system. First, scavenging tests were carried out to get further insights into the nature of the reactive oxidizing species formed upon activation of PS. Then, catalytic experiments were conducted with thermally modified rGO materials to elucidate the oxygen-containing surface groups involved in PS activation. By considering the information obtained in these experiments (i.e., the apparently dominant reactive species formed upon PS activation and the rGO catalytic site where most likely this activation takes place), a mechanism for the rGO-PS oxidation process was finally suggested.

According to the previous literature, it can be assumed that the strong oxidants potentially generated in the rGO-PS process may be HO•, $SO_4^{\bullet -}$ and $^1O_2$ [21,22,24,30]. Their relative contributions to organic pollutants oxidation can be elucidated if a selective removal of these species from the reaction medium is achieved. Under this premise, the study of the oxidizing species responsible for pollutants degradation in the rGO-PS system was conducted by means of batch catalytic experiments with addition of different scavengers, namely *tert*-butanol (tBuOH), methanol (MeOH) and furfuryl alcohol (FFA). Ph was employed as model pollutant. The scavenger approach is a well-established method in environmental catalysis studies to investigate the relative role of the different oxidizing species in pollutants abatement. It can be used alone or in combination with other more sophisticated techniques designed with similar purposes [24,26,42,43]. Results are given in Fig. 5.

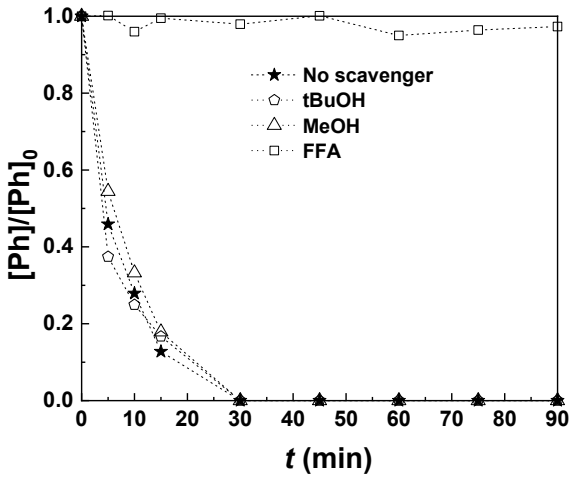

Figure 5. Catalytic oxidation of Ph via batch rGO-PS process in the presence of various scavengers. $[Ph]_0$ = 5 mg L^{-1}, $[rGO]_0$ = 0.25 g L^{-1}, $[PS]_0$ = 0.25 mM, $[tBuOH]_0 = [MeOH]_0 = [FFA]_0$ = 100 mM, and pH_0 = 7.0 (inherent pH).

Ph degradation profiles observed in experiments with tBuOH and MeOH addition were almost identical to that obtained in the assay performed in the absence of scavengers. The only exception was found in the experiment conducted with FFA, for which the abatement of the model compound was completely inhibited. tBuOH reacts fast with HO• ($k_{tBuOH, HO•}$ = $6 \cdot 10^8$ M^{-1} s^{-1} [44]), whereas it presents markedly slower kinetics with $SO_4^{•-}$ ($k_{tBuOH,SO4•-}$ = $9 \cdot 10^5$ M^{-1} s^{-1} [45]). On its part, $SO_4^{•-}$ was suppressed by adding MeOH ($k_{MeOH,SO4•-}$= $2 \cdot 10^7$ M^{-1} s^{-1} [45]), which also reacts fast with HO• ($k_{MeOH, HO•}$ = $9.7 \cdot 10^8$ M^{-1} s^{-1} [44]). Moreover, $^1O_2$ reactions with tBuOH and MeOH are slow ([46], rate constant value not available). Finally, FFA undergoes fast reaction with $^1O_2$ ($k_{FFA,1O2}$ = $1.2 \cdot 10^8$ M^{-1} s^{-1} [46]), although this alcohol also presents a high reactivity towards HO• ($k_{FFA, HO•}$ = $1.5 \cdot 10^{10}$ M^{-1} s^{-1} [44]) and most probably also with $SO_4^{•-}$ (kinetic data not found). This analysis and the results obtained point towards a dominant role of $^1O_2$ in the rGO-PS system. Either way, these indications could constitute a step further in the elucidation of the oxidation mechanisms governing the rGO-PS process, especially in view of other

works dealing with related catalytic systems (e.g., rGO or commercial graphene combined with PMS [24,30]) in which a non-radical oxidation mechanism was suggested to be relevant but the specific role of $^1O_2$ was not discussed or clearly identified. More importantly, our results are in contrast with conclusions drawn in the few previous works studying the same process (i.e., rGO-PS), where the oxidation of organic compounds has been primarily attributed to $SO_4^{\bullet-}$ [22] or $HO^{\bullet}$ [21]. In addition to potential differences in the composition of the employed catalysts, none of these two previous works assessed the potential contribution of $^1O_2$ in the overall degradation of the model pollutants, thus underestimating the role of this non-radical pathway. In this sense, the present study is the first one providing experimental data suggesting the potentially important role of $^1O_2$ in the rGO-PS oxidation system.

The following experiments were performed in order to assess which are the most likely active sites at the surface of rGO, i.e., where activation and subsequent formation of oxidizing species (i.e., $^1O_2$, according to the above results) takes place. To that end, rGO derivatives prepared by thermal treatment at different temperatures (*i.e.*, rGO-500, rGO-850 and rGO-1000) were used as catalysts in additional batch tests, employing Ph as model pollutant. In this case, the initial concentration of Ph was raised from 5 to 30 mg L^{-1}, making the process slower in such a way that differences in the treatment performance (i.e., kinetics) with different catalysts could be more clearly observed. The resulting Ph abatement curves are shown in Fig. 6a. Data obtained in adsorption tests conducted with the same materials can be found in Fig. S11, and indicate only a slight variation (± 10%) in the Ph adsorption levels compared to pristine rGO, in all cases.

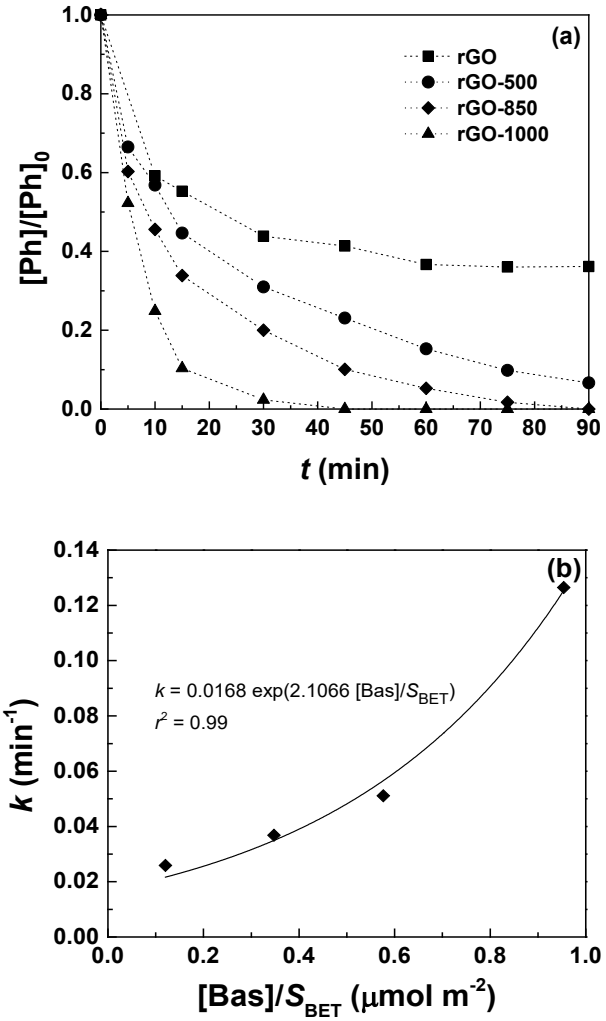

Figure 6. Catalytic oxidation of phenol in batch rGO-PS experiments with pristine and thermally treated rGO at different temperatures. a) Degradation profiles; b) Dependence of pseudo first order rate constant for Ph degradation with the S_{BET}-normalized concentration of oxygen basic surface groups ([Bas]/S_{BET}). $[Ph]_0$ = 30 mg L^{-1}, $[rGO]_0$ = 0.25 g L^{-1}, $[PS]_0$ = 1 mM, and pH_0 = 7.0 (inherent pH).

As observed in Fig 6a, the degradation of Ph is faster when employing rGO derivatives prepared with increasing treatment temperatures. The negative correlation between surface oxygen content and treatment temperature (Fig. 1a) confirms the inverse trend between catalytic activity and the oxygen percentage, as already suggested in previous studies on PS and PMS activation by rGO materials [20,21,30,31]. Moreover, TPD data obtained in this study for the tested materials provide a plausible explanation to this

correlation. As discussed, reduction of the overall surface oxygen content in rGO upon thermal treatment at increasing temperatures is accompanied by a progressive shift in the type of functionalities, from acidic to basic (Tables S4-S6). Accordingly, the fact that decreasing the oxygen contents to very low percent values results in a significant improvement of the catalytic activity might be explained by two different phenomena, though partly related and in fact simultaneous. On one hand, acidic oxygen-containing functionalities, like SA and LA, may hinder PS activation by causing an electron-withdrawing effect at rGO reactive centers [47,48]. At the same time, a rise in the concentration of more basic, and electron donor oxygen-containing groups such as CQ and Bas, could increase the possibility of electron-transfer or nucleophilic reactions with PS, resulting in a faster activation of this molecule and subsequent pollutant oxidation [47,48]. The positive influence of basic groups becomes particularly evident when plotting the pseudo first order rate constant of phenol degradation against [Bas]/S_{BET} (Fig. 6b). The observed exponential correlation suggests a strong dependence of rGO activity with the concentration of the most basic surface oxygen functionalities. Some of these, such as pyrone moieties, contain carbonyl functions (C=O) which have been suggested to be important PMS activation sites in carbon nanomaterials [31,32]. In this respect, another work showed that simple molecules containing carbonyl groups can also activate PMS [49]. The fact that rGO-1000 performed better as a catalyst than rGO-850 constitutes a strong evidence for the important role of basic carbonyl-containing moieties in the rGO-PS mechanism. As seen in Tables S4 and S5, only CQ and Bas surface functionalities were present, being the concentration of Bas groups 41% higher in the case of rGO-1000. The amount of CQ groups, on its part, was reduced by 77% from rGO-850 to rGO-1000. These results provide novel insights on the nature of rGO catalytic sites, which support the role of surface carbonyl groups in PS activation. However, these data also suggest

that, even though the presence of C=O groups is apparently necessary to trigger PS activation, the basicity of carbonyl-containing reactive centers appears to play a key role in the process. In this respect, pyrone-like moieties are, for the first time, suggested to be the main activation sites for PS in rGO. Furthermore, these results point out the possibilities of a simple yet powerful method (i.e., thermal treatment) for potential tuning of the rGO surface chemistry, through an increase in the relative amount of pyrone-like functions.

Indications about the potentially dominant role of $^1O_2$ and pyrone-like moieties as main reactive sites were put together in order to propose a mechanism for PS activation by rGO. Any involvement of dissolved oxygen in $^1O_2$ formation was discarded through performing an additional batch experiment under N_2 bubbling (Fig. S12). From previous investigations, it is widely accepted that PMS can react with simple ketones [50] and quinones [49] to yield $^1O_2$, which has been detected by spectroscopic methods [50]. This reaction has been suggested to proceed with formation of a dioxirane intermediate that decays rapidly in the presence of PMS [50,51]. Thus, a similar activation mechanism can take place in the rGO-PS system. The proposed mechanism is schematically depicted in Fig. 7, with pyrone-like moieties represented by one of the most basic species [52]. According to this reaction pathway, PS activation by rGO proceeds mainly via nucleophilic addition of this molecule to the carbonyl group of pyrone-like functions, forming the dioxirane intermediate (shown between brackets) and sulfate anions. Nucleophilic attack of this transient species with another PS molecule would yield $^1O_2$ and further sulfate anions, in addition to allowing the recovery of the initial ketone group. The symmetrical charge distribution of the peroxide bond in PS makes this type of nucleophilic reaction somewhat more complicated compared to that described for PMS,

which has an asymmetrical O-O bond. Still, it appears to be possible according to relatively recent reports [53].

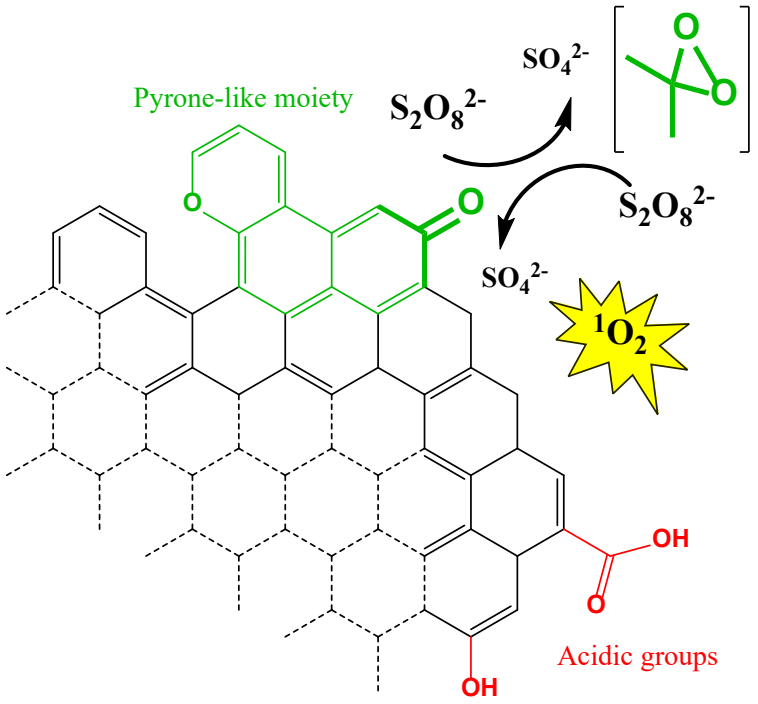

Figure 7. Schematic representation of the proposed mechanisms for $^1O_2$ production upon PS activation on pyrone-like moieties at the surface of rGO.

Conclusions

Unmodified, commercial rGO is effective for the fabrication of PTFE-supported catalytic membranes designed for PS activation and abatement of water organic pollutants in continuous mode of operation. The performance of this process was found to increase as the water flow rate decreases and the supported catalyst load increases. The efficiency in organic contaminant oxidation is comparable to those obtained in previous studies performed with metal-free, carbon-based catalytic membranes fabricated with heteroatom doped or composite materials whose preparation usually involve energy- and time-

consuming procedures. The use of rGO, a relatively easier material to synthesize, may thus entail important savings in the membrane fabrication methodology.

Concerning the catalytic stability of the PTFE-supported rGO membrane, a dramatic drop in the catalytic activity was observed after the first 2-3 days of operation. Nevertheless, simple thermal regeneration procedures are suitable to recover its catalytic activity.

With regard to the mechanisms governing PS activation and subsequent removal of water organic pollutants, the presence of basic oxygen-containing surface functionalities on rGO, mainly pyrone-like moieties, was shown to be particularly relevant for the decomposition of PS via formation of $^1O_2$ (i.e., the main oxidizing species in the rGO-PS system). Accordingly, a reaction mechanism was proposed based on PS nucleophilic attack on C=O moieties at the surface of rGO.

Acknowledgements

This work was financially supported by project NORTE-01-0145-FEDER-031049 (InSpeCt - PTDC/EAM-AMB/31049/2017) funded by FEDER funds through NORTE 2020 - Programa Operacional Regional do NORTE, and by national funds (PIDDAC) through FCT/MCTES. We would also like to thank the scientific collaboration under Base Funding - UIDP/50020/2020 of the Associate Laboratory LSRE-LCM - funded by national funds through FCT/MCTES (PIDDAC). AC and NL are grateful to the Spanish Government for their postdoctoral (BES-2015-074109, POP stage) and PhD (FPU-16/02101) fellowships, respectively.

References

[1]S. Wu, H. He, X. Li, C. Yang, G. Zeng, B. Wu, S. He, L. Lu, Insights into atrazine degradation by persulfate activation using composite of nanoscale zero-valent iron and graphene: Performances and mechanisms, Chem. Eng. J. 341 (2018) 126–136. https://doi.org/10.1016/j.cej.2018.01.136.

[2]R. Xiao, Z. Luo, Z. Wei, S. Luo, R. Spinney, W. Yang, D.D. Dionysiou, Activation of peroxymonosulfate/persulfate by nanomaterials for sulfate radical-based advanced oxidation technologies, Curr. Opin. Chem. Eng. 19 (2018) 51–58. https://doi.org/10.1016/j.coche.2017.12.005.

[3]S.F. Zhang, H. Li, C. Hou, L.N. Liu, Y. Wang, M.K. Zhao, C. Liang, Recyclable ZIF-9@CA-Fe3O4/RGO/cellulose composite membrane as efficient catalysts for activating peroxymonosulfate to degrade methylene blue, Cellulose. 27 (2020) 3287–3300. https://doi.org/10.1007/s10570-020-02998-x.

[4]C. Zhu, F. Liu, C. Ling, H. Jiang, H. Wu, A. Li, Growth of graphene-supported hollow cobalt sulfide nanocrystals via MOF-templated ligand exchange as surface-bound radical sinks for highly efficient bisphenol A degradation, Appl. Catal. B Environ. 242 (2019) 238–248. https://doi.org/10.1016/j.apcatb.2018.09.088.

[5]N. Svage, Super carbon, Nature. 483 (2012) 30–31.

[6]X. Duan, Z. Ao, H. Sun, S. Indrawirawan, Y. Wang, J. Kang, F. Liang, Z.H. Zhu, S. Wang, Nitrogen-doped graphene for generation and evolution of reactive radicals by metal-free catalysis, ACS Appl. Mater. Interfaces. 7 (2015) 4169–4178. https://doi.org/10.1021/am508416n.

[7]S. Indrawirawan, H. Sun, X. Duan, S. Wang, Low temperature combustion synthesis of nitrogen-doped graphene for metal-free catalytic oxidation, J. Mater. Chem. A. 3 (2015) 3432–3440. https://doi.org/10.1039/c4ta05940a.

[8]X. Wang, Y. Qin, L. Zhu, H. Tang, Nitrogen-doped reduced graphene oxide as a

bifunctional material for removing bisphenols: Synergistic effect between adsorption and catalysis, Environ. Sci. Technol. 49 (2015) 6855–6864. https://doi.org/10.1021/acs.est.5b01059.

[9]X. Chen, T.T. Lim, Highly-efficient peroxymonosulfate activation for sulfacetamide degradation over nitrogen-functionalized graphene: The effect of thermal annealing temperature on reactive functional groups, Chem. Eng. Trans. 73 (2019) 145–150. https://doi.org/10.3303/CET1973025.

[10] H. Chen, K.C. Carroll, Metal-free catalysis of persulfate activation and organic-pollutant degradation by nitrogen-doped graphene and aminated graphene, Environ. Pollut. 215 (2016) 96–102. https://doi.org/10.1016/j.envpol.2016.04.088.

[11] D. Li, X. Duan, H. Sun, J. Kang, H. Zhang, M.O. Tade, S. Wang, Facile synthesis of nitrogen-doped graphene via low-temperature pyrolysis: The effects of precursors and annealing ambience on metal-free catalytic oxidation, Carbon. 115 (2017) 649–658. https://doi.org/10.1016/j.carbon.2017.01.058.

[12] J. Kang, L. Zhou, X. Duan, H. Sun, S. Wang, Catalytic degradation of antibiotics by metal-free catalysis over nitrogen-doped graphene, Catal. Today. (2018) 0–1. https://doi.org/10.1016/j.cattod.2018.12.002.

[13] X. Chen, W. Da Oh, Z.T. Hu, Y.M. Sun, R.D. Webster, S.Z. Li, T.T. Lim, Enhancing sulfacetamide degradation by peroxymonosulfate activation with N-doped graphene produced through delicately-controlled nitrogen functionalization via tweaking thermal annealing processes, Appl. Catal. B Environ. 225 (2018) 243–257. https://doi.org/10.1016/j.apcatb.2017.11.071.

[14] P. Sun, H. Liu, Z. Zhai, X. Zhang, Y. Fang, J. Tan, J. Wu, Degradation of UV filter BP-1 with nitrogen-doped industrial graphene as a metal-free catalyst of peroxymonosulfate activation, Chem. Eng. J. 356 (2019) 262–271.

https://doi.org/10.1016/j.cej.2018.09.023.

[15] J. Kang, X. Duan, L. Zhou, H. Sun, M.O. Tadé, S. Wang, Carbocatalytic activation of persulfate for removal of antibiotics in water solutions, Chem. Eng. J. 288 (2016) 399–405. https://doi.org/10.1016/j.cej.2015.12.040.

[16] Q. Wang, L. Li, L. Luo, Y. Yang, Z. Yang, H. Li, Y. Zhou, Activation of persulfate with dual-doped reduced graphene oxide for degradation of alkylphenols, Chem. Eng. J. 376 (2019) 120891. https://doi.org/10.1016/j.cej.2019.01.170.

[17] X. Duan, K. O'Donnell, H. Sun, Y. Wang, S. Wang, Sulfur and Nitrogen Co-Doped Graphene for Metal-Free Catalytic Oxidation Reactions, Small. 11 (2015) 3036–3044. https://doi.org/10.1002/smll.201403715.

[18] P. Sun, H. Liu, M. Feng, L. Guo, Z. Zhai, Y. Fang, X. Zhang, V.K. Sharma, Nitrogen-sulfur co-doped industrial graphene as an efficient peroxymonosulfate activator: Singlet oxygen-dominated catalytic degradation of organic contaminants, Appl. Catal. B Environ. 251 (2019) 335–345. https://doi.org/10.1016/j.apcatb.2019.03.085.

[19] H. Sun, Y. Wang, S. Liu, L. Ge, L. Wang, Z. Zhu, S. Wang, Facile synthesis of nitrogen doped reduced graphene oxide as a superior metal-free catalyst for oxidation, Chem. Commun. 49 (2013) 9914–9916. https://doi.org/10.1039/c3cc43401j.

[20] H. Sun, S. Liu, G. Zhou, H.M. Ang, M.O. Tadé, S. Wang, Reduced graphene oxide for catalytic oxidation of aqueous organic pollutants, ACS Appl. Mater. Interfaces. 4 (2012) 5466–5471. https://doi.org/10.1021/am301372d.

[21] X. Duan, H. Sun, J. Kang, Y. Wang, S. Indrawirawan, S. Wang, Insights into Heterogeneous Catalysis of Persulfate Activation on Dimensional-Structured Nanocarbons, ACS Catal. 5 (2015) 4629–4636.

https://doi.org/10.1021/acscatal.5b00774.

[22] T. Olmez-Hanci, I. Arslan-Alaton, S. Gurmen, I. Gafarli, S. Khoei, S. Safaltin, D. Yesiltepe Ozcelik, Oxidative degradation of Bisphenol A by carbocatalytic activation of persulfate and peroxymonosulfate with reduced graphene oxide, J. Hazard. Mater. 360 (2018) 141–149. https://doi.org/10.1016/j.jhazmat.2018.07.098.

[23] S. Wang, J. Wang, Kinetics of PMS activation by graphene oxide and biochar, Chemosphere. 239 (2020) 124812. https://doi.org/10.1016/j.chemosphere.2019.124812.

[24] R.R. Solís, I.F. Mena, M.N. Nadagouda, D.D. Dionysiou, Adsorptive interaction of peroxymonosulfate with graphene and catalytic assessment via non-radical pathway for the removal of aqueous pharmaceuticals, J. Hazard. Mater. 384 (2020) 121340. https://doi.org/10.1016/j.jhazmat.2019.121340.

[25] Y. Liu, L. Yu, C.N. Ong, J. Xie, Nitrogen-doped graphene nanosheets as reactive water purification membranes, Nano Res. 9 (2016) 1983–1993. https://doi.org/10.1007/s12274-016-1089-7.

[26] M. Pedrosa, G. Drazic, P.B. Tavares, J.L. Figueiredo, A.M.T. Silva, Metal-free graphene-based catalytic membrane for degradation of organic contaminants by persulfate activation, Chem. Eng. J. 369 (2019) 223–232. https://doi.org/10.1016/j.cej.2019.02.211.

[27] O. Vieira, R.S. Ribeiro, M. Pedrosa, A.R. Lado Ribeiro, A.M.T. Silva, Nitrogen-doped reduced graphene oxide – PVDF nanocomposite membrane for persulfate activation and degradation of water organic micropollutants, Chem. Eng. J. 402 (2020) 126117. https://doi.org/10.1016/j.cej.2020.126117.

[28] J. Sheng, H. Yin, F. Qian, H. Huang, S. Gao, J. Wang, Reduced graphene oxide-

based composite membranes for in-situ catalytic oxidation of sulfamethoxazole operated in membrane filtration, Sep. Purif. Technol. 236 (2020) 116275. https://doi.org/10.1016/j.seppur.2019.116275.

[29] D.X. Luong, K. V. Bets, W.A. Algozeeb, M.G. Stanford, C. Kittrell, W. Chen, R. V. Salvatierra, M. Ren, E.A. McHugh, P.A. Advincula, Z. Wang, M. Bhatt, H. Guo, V. Mancevski, R. Shahsavari, B.I. Yakobson, J.M. Tour, Gram-scale bottom-up flash graphene synthesis, Nature. 577 (2020) 647–651. https://doi.org/10.1038/s41586-020-1938-0.

[30] X. Duan, Z. Ao, L. Zhou, H. Sun, G. Wang, S. Wang, Occurrence of radical and nonradical pathways from carbocatalysts for aqueous and nonaqueous catalytic oxidation, Appl. Catal. B Environ. 188 (2016) 98–105. https://doi.org/10.1016/j.apcatb.2016.01.059.

[31] X. Duan, H. Sun, Z. Ao, L. Zhou, G. Wang, S. Wang, Unveiling the active sites of graphene-catalyzed peroxymonosulfate activation, Carbon. 107 (2016) 371–378. https://doi.org/10.1016/j.carbon.2016.06.016.

[32] Y. Wang, Z. Ao, H. Sun, X. Duan, S. Wang, Activation of peroxymonosulfate by carbonaceous oxygen groups: Experimental and density functional theory calculations, Appl. Catal. B Environ. 198 (2016) 295–302. https://doi.org/10.1016/j.apcatb.2016.05.075.

[33] L. Sbardella, I.V. Gala, J. Comas, S.M. Carbonell, I. Rodríguez-Roda, W. Gernjak, Integrated assessment of sulfate-based AOPs for pharmaceutical active compound removal from wastewater, J. Clean. Prod. 260 (2020) 121014. https://doi.org/10.1016/j.jclepro.2020.121014.

[34] S. Wacławek, H. V. Lutze, K. Grübel, V.V.T. Padil, M. Černík, D.D. Dionysiou, Chemistry of persulfates in water and wastewater treatment: A review, Chem. Eng.

J. 330 (2017) 44–62. https://doi.org/10.1016/j.cej.2017.07.132.

[35] R.S. Ribeiro, Z. Frontistis, D. Mantzavinos, D. Venieri, M. Antonopoulou, I. Konstantinou, A.M.T. Silva, J.L. Faria, H.T. Gomes, Magnetic carbon xerogels for the catalytic wet peroxide oxidation of sulfamethoxazole in environmentally relevant water matrices, Appl. Catal. B Environ. 199 (2016) 170–186. https://doi.org/10.1016/j.apcatb.2016.06.021.

[36] Modification of the surface chemistry of activated carbons, Carbon. 37 (1999) 1379–1389. https://doi.org/10.1016/S0008-6223(98)00333-9.

[37] J.L. Figueiredo, M.F.R. Pereira, M.M.A. Freitas, J.J.M. Órfão, Characterization of active sites on carbon catalysts, Ind. Eng. Chem. Res. 46 (2007) 4110–4115. https://doi.org/10.1021/ie061071v.

[38] A.H. Lima, J.P. Mendonça, M. Duarte, F. Stavale, C. Legnani, G.S.G. De Carvalho, I.O. Maciel, F. Sato, B. Fragneaud, W.G. Quirino, Reduced graphene oxide prepared at low temperature thermal treatment as transparent conductors for organic electronic applications, Org. Electron. 49 (2017) 165–173. https://doi.org/10.1016/j.orgel.2017.05.054.

[39] L. Song, F. Khoerunnisa, W. Gao, W. Dou, T. Hayashi, K. Kaneko, M. Endo, P.M. Ajayan, Effect of high-temperature thermal treatment on the structure and adsorption properties of reduced graphene oxide, Carbon. 52 (2013) 608–612. https://doi.org/10.1016/j.carbon.2012.09.060.

[40] A. Bagri, C. Mattevi, M. Acik, Y.J. Chabal, M. Chhowalla, V.B. Shenoy, Structural evolution during the reduction of chemically derived graphene oxide, Nat. Chem. 2 (2010) 581–587. https://doi.org/10.1038/nchem.686.

[41] European Commission, Decision (EU) 2020/1161 of 4 August 2020 establishing a watch list of substances for Union-wide monitoring in the field of water policy

pursuant to Directive 2008/105/EC of the European Parliament and of the Council, Off. J. Eur. Union. L 257 (2020) 32–35.

[42] S. Wu, H. Liu, C. Yang, X. Li, Y. Lin, K. Yin, J. Sun, Q. Teng, C. Du, Y. Zhong, High-performance porous carbon catalysts doped by iron and nitrogen for degradation of bisphenol F via peroxymonosulfate activation, Chem. Eng. J. 392 (2020) 123683. https://doi.org/10.1016/j.cej.2019.123683.

[43] S. Wu, H. Liu, Y. Lin, C. Yang, W. Lou, J. Sun, C. Du, D. Zhang, L. Nie, K. Yin, Y. Zhong, Insights into mechanisms of UV/ferrate oxidation for degradation of phenolic pollutants: Role of superoxide radicals, Chemosphere. 244 (2020) 125490. https://doi.org/10.1016/j.chemosphere.2019.125490.

[44] G. V Buxton, C.L. Greenstock, W.P. Helman, A.B. Ross, Critical Review of rate constants for reactions of hydrated electrons, hydrogen atoms and hydroxyl radicals in aqueous solution, J. Phys. Chem. Ref. Data. 17 (1988) 513–886. https://doi.org/10.1063/1.555805.

[45] R.E. Huie, P. Neta, A.B. Ross, Rate Constants for Reactions of Inorganic Radicals in Aqueous Solution, J. Phys. Chem. Ref. Data. 17 (1988) 709–1050. https://doi.org/10.1063/1.555978.

[46] F. Wilkinson, J.G. Brummer, Rate constants for the decay and reactions of the lowest electronically excited singlet state of molecular oxygen in solution, J. Phys. Chem. Ref. Data. 10 (1981) 809–999. https://doi.org/10.1063/1.555655.

[47] X. Chen, W. Oh, T. Lim, Graphene- and CNTs-based carbocatalysts in persulfates activation : Material design and catalytic mechanisms, Chem. Eng. J. 354 (2018) 941–976. https://doi.org/10.1016/j.cej.2018.08.049.

[48] C. Han, X. Duan, M. Zhang, W. Fu, X. Duan, W. Ma, S. Liu, S. Wang, X. Zhou, Role of electronic properties in partition of radical and nonradical processes of

carbocatalysis toward peroxymonosulfate activation, Carbon. 153 (2019) 73–80. https://doi.org/10.1016/j.carbon.2019.06.107.

[49] Y. Zhou, J. Jiang, Y. Gao, J. Ma, S.Y. Pang, J. Li, X.T. Lu, L.P. Yuan, Activation of Peroxymonosulfate by Benzoquinone: A Novel Nonradical Oxidation Process, Environ. Sci. Technol. 49 (2015) 12941–12950. https://doi.org/10.1021/acs.est.5b03595.

[50] A. Lange, H. Brauer, On the formation of dioxiranes and of singlet oxygen by the ketone-catalysed decomposition of Caro's acid, J. Chem. Soc. Perkin Trans. 2. 2 (1996) 805–811.

[51] J.O. Edwards, R.H. Pater, R. Curci, F. Di Furia, On the formation and reactivity of dioxirane intermediates in the reaction of peroxoanions with organic substrates, Photochem. Photobiol. 30 (1979) 63–70.

[52] E. Fuente, J.A. Menéndez, D. Suárez, M.A. Montes-Morán, Basic surface oxides on carbon materials: A global view, Langmuir. 19 (2003) 3505–3511. https://doi.org/10.1021/la026778a.

[53] X. Cheng, H. Guo, Y. Zhang, X. Wu, Y. Liu, Non-photochemical production of singlet oxygen via activation of persulfate by carbon nanotubes, Water Res. 113 (2017) 80–88. https://doi.org/10.1016/j.watres.2017.02.016.